Journal of Inorganic Biochemistry 195 (2019) 51–60

Contents lists available at ScienceDirect

Journal of Inorganic Biochemistry

journal homepage: www.elsevier.com/locate/jinorgbio

Studying the reactivity of “old” Cu(II) complexes for “novel” anticancer purposes

Quim Peña[a,b], Julia Lorenzo[c], Giuseppe Sciortino[a], Sergi Rodríguez-Calado[c], Jean-Didier Maréchal[a], Pau Bayón[a], A. Jalila Simaan[b], Olga Iranzo[b], Mercè Capdevila[a], Òscar Palacios[a,*]

[a] Departament de Química, Facultat de Ciències, Universitat Autònoma de Barcelona, 08193-Cerdanyola del Vallès, Barcelona, Spain
[b] Aix Marseille Univ, CNRS, Centrale Marseille, iSm2, Marseille, France
[c] Institut de Biotecnologia i Biomedicina, Dept. Bioquímica i Biologia Molecular, Universitat Autònoma de Barcelona, 08193-Cerdanyola del Vallès, Barcelona, Spain

A B S T R A C T

Reactive oxygen species (ROS) formation appears as one of the most promising pathways to induce cell death. The interesting Cu(II)/Cu(I) redox pair has been reported to biologically generate ROS and induce cell damage. Simple metal complexes, such as cisplatin, sometimes offer even better properties than others highly accurately synthesized, which imply considerable time and economical efforts. This work relies on the synthesis and characterisation of four existing Cu(II) complexes bearing *N*-donor ligands, previously used for a totally different intend, but tested now for anticancer purposes. Furthermore, a relationship between their coordinating features, *i.e.* their redox behaviour, with their biological activity have been inferred to further understand the medicinal role of the Cu(II)/Cu(I) redox pair. Cytotoxicity studies and interactions towards DNA have been assessed, studying both covalent and non-covalent modes of binding *via* mass spectrometry (MS), UV–Vis and fluorescence, evaluating the cleaving properties of the assayed compounds, as well as their capacity to generate ROS inside the cells. The role of the ligand for one of the complexes has been evaluated by a computational approach. The idea of using “old” complexes for “novel” anticancer purposes can offer promising results in the future, being a simple but interesting approach to study, as we demonstrate here for most of the complexes analysed, showing a non-expected “new” and beneficial role.

1. Introduction

The discovery of cisplatin placed Medicinal Inorganic Chemistry in front of the fight against cancer and stimulated the research on other similar platinum compounds such as oxaliplatin, carboplatin and nedaplatin [1–3]. Nonetheless, and despite the fact that some of them are still widely applied, the use of Pt-compounds have been limited owing to several undesired side-effects, intrinsic resistance, and the loss of effectiveness due to their strong interaction with different biomolecules, such as glutathione (GSH) or metallothioneins (MTs) [4–7]. In this scenario, non-Pt drugs emerged about 30 years ago to improve the properties of Pt-complexes, and to avoid the drawbacks associated with Pt-drugs. Ru, Ir, Au, Ti, or Pd are some of the metals whose complexes have been tested as anticancer compounds, exhibiting promising results in most cases [8–12]. Metals and their inorganic complexes show an enormous versatility in front of strictly organic compounds. The possibility of having several oxidation states, different coordination numbers and diverse geometries gives rise to a broader spectrum of properties to be tuned [13]. Among them, Cu complexes have become promising alternatives for cancer treatment during the last decade [14–18].

Copper is an essential biometal, being widely present in many biomolecules and playing a remarkable role in a diversity of biochemical processes, partially due to its interesting Cu(II)/Cu(I) redox pair [19–21]. In fact, one of the main potentialities of Cu as antiproliferative agent lays on its capability to form reactive oxygen species (ROS) inside the cells [22]. The generation of these reactive species is not only reported to damage DNA, but also to offer a putative discrimination between healthy and non-healthy cells [23,24]. Considering that cancer cells exhibit abnormal levels of ROS and that they show higher vulnerability to ROS level changes than healthy cells do, it is assumed that alteration of those levels may be a unique opportunity to selectively target cancer cells [23,24]. Therefore, understanding and providing new insights into the mechanisms of ROS generation by Cu(II) complexes appear to be indispensable.

Cu(II) complexes have been used since long for different applications, specially related to catalysis [25–30]. Moreover, the design and synthesis of chelating ligands for Cu(II) in the treatment of the Alzheimer's disease is also a current topic of interest [31–33]. However, and based on both the fact that one of the most effective

* Corresponding author.
E-mail address: oscar.palacios@uab.cat (Ò. Palacios).

https://doi.org/10.1016/j.jinorgbio.2019.03.011
Received 6 November 2018; Received in revised form 12 March 2019; Accepted 14 March 2019
Available online 18 March 2019

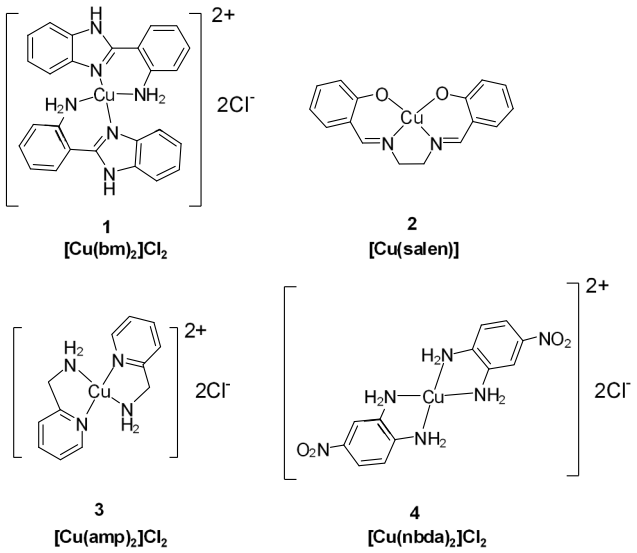

Fig. 1. Chemical structures for the complexes **1–4**. The ligands are: 2-(2-aminophenyl)-1*H*-benzimidazole (bm); *N,N′*-bis(salicylidene)ethylenediamine ($salenH_2$); 2-(aminomethyl)pyridine (amp); and 4-nitrobenzene-1,2-diamine (nbda).

chemotherapeutic agents is cisplatin –a highly simple complex- and on the potentiality of ROS production by copper, many "old" Cu(II) complexes may offer unknown and interesting antiproliferative activities. Cu(II) complexes bearing N-donor ligands have acquired strong importance due to the stability of Cu—N bonds and the promising cytotoxic effect reported by *N*-heteroaromatic planar groups, due to their efficient DNA binding/intercalating action and to increase the affinity of Cu to DNA [16,34].

2. Results and discussion

In this work, four different Cu(II) complexes (**1–4**, Fig. 1) have been selected to study their reactivity as putative anticancer compounds. Those have been selected following several criteria: i) small/simple molecules; ii) bearing *N*-donor ligands and planar aromatic moieties; iii) used for other purposes than anticancer agents (catalysis, Alzheimer's disease, *etc.*) [32,35–37]. The interest is twofold. On one side, the presence of *N*-heteroaromatic planar scaffolds promote efficient DNA binding/intercalating action and cleaving properties [16,34]. On the other hand, the use of these redox-active ligands (*o*-phenylenediamine derivatives and other π-conjugated aromatic coordinating scaffolds) has attracted considerable attention. Their versatility to expand the electron transfer reactivity of the coordinated metals beyond the mere inherent metal activity is interesting in terms of potential redox-mediated anticancer pathways, *i.e.* ROS generation [38].

The synthesis of the Cu(II) complexes 1–4 was carried out following previous works [32,35,37,39]. They were characterized by ESI-MS, elemental analysis and EPR (Figs. S1 and S2) in order to confirm the integrity of the species formed. All our experimental data are in agreement with the reported structures (Fig. 1). Complexes 1, 2 and 3 maintain their coordination structure in dimethyl sulfoxide (dmso) solution and mainly exist in single square-planar conformations. In the case of complex 4, ESI-MS and EPR data (Fig. S2) suggest the presence of two different compounds in dmso: a major species with N_2O_2 coordination environment and a minor one with O_4 environment, both adopting a partial distorted configuration from planarity [40,41]. The peak associated to the $[Cu(nbda)_2]^{2+}$ expected species (m/z = 368.0273) was only detected in pure methanol (MeOH). This suggests a solvent-dependent process involving partial ligand release from complex 4 and leading to the $[Cu(nbda)]^{2+}$ species (m/z = 214.9795).

Table 1
IC_{50} (μM) values at 24 h of complexes **1–4** and their corresponding ligands in HeLa, MCF7 and CCD112CoN cultures, using $CuCl_2{\cdot}2H_2O$ as reference compound. The results shown are representative of at least three independent experiments (N = 3).

Compound	HeLa	MCF7	CCD112CoN
1	87 ± 6	93 ± 8	n.d.
2	n.d.	n.d.	n.d.
3	48 ± 8	69 ± 6	68 ± 4
4	23 ± 5	5 ± 3	58 ± 7
Ligand 1 (bm)	n.d.	n.d.	n.d.
Ligand 2 (salen)	n.d.	n.d.	n.d.
Ligand 3 (amp)	n.d.	n.d.	n.d.
Ligand 4 (nbda)	n.d.	n.d.	n.d.
$CuCl_2{\cdot}2H_2O$	n.d.	n.d.	n.d.

n.d. (non determined). IC_{50} not able to be determined. These cases are those whose dose-response curve does not reach the 0% of viability at 200 μM (Fig. S3).

Further efforts have been devoted to rationalise the species here formed with a theoretical approach (see following sections).

The reactivity of the complexes **1–4** has been investigated in order to correlate their chemical characteristics with their antiproliferative activity.

2.1. Cytotoxicity assays

In vitro anti-proliferative activity of the complexes **1–4** and that of their corresponding free ligands was determined on HeLa and MCF7 cell lines. The IC_{50} values and the cell-inhibition profiles are summarised in Table 1 and Fig. S3. Remarkably, all ligands, as well as $CuCl_2$ and complex **2** exhibit poor or negligible antiproliferative activity in the two cancer cell lines, whereas complexes **1**, **3**, and **4** show significant and dose-dependent cytotoxicity when compared to $CuCl_2$ and cisplatin ($IC_{50,24h}$ of 40 μM in HeLa and of 38 μM in MCF7) [42] in both cancer cell lines. According to the IC_{50} values, their cytotoxicity in HeLa and MCF7 can be ordered as **4** > **3** > **1** ≫ **2**. Complexes **3** and **4** have the lowest IC_{50} values, thus being the most active ones. Indeed, after 24 h of treatment, both complexes trigger cell death at similar and even lower concentrations as that found for the reference compound cisplatin (40 μM) in HeLa cell lines. The dose-response curve of the cell-viability diagrams shows that complexes **1** and **3** have a higher toxicity in HeLa than in MCF7 cell lines. Interestingly, complex **4** deserves special attention since it represents a significant improvement in terms of cytotoxicity with respect to cisplatin both in HeLa and MCF7 lines. Particularly, its IC_{50} in MCF7 (Table 1) is about 10 times lower than that found for cisplatin (38 μM) [42], pointing to a promising compound to treat breast cancer (Fig. S3).

Cytotoxicity of complexes **1–4** in normal colon fibroblasts (CDD112CoN cell line) have been also tested as a proof-of-concept reference of non-cancer cells. As observed in the dose-response cell viability diagrams (Fig. S3), all the complexes exhibit lower (complexes **1**, **2** and **4**) or similar (complex **3**) toxicity in fibroblasts with respect to both cancer HeLa and MCF7 cell lines. Significant and interesting differences can be observed in complex **4**, the most active one, whose IC_{50} value in HeLa and MCF7 is two and nine-fold lower, respectively, than the corresponding value in fibroblasts. This may provide less side-effects, which could represent an advantage for future *in vivo* tests.

The antiproliferative activity of complexes **1**, **3**, and **4** can only be attributed to a conjoint contribution between the ligand and the Cu(II) ion, *i.e.* to the entire complex, and not solely to the simple addition of the Cu(II) ion plus the ligands cytotoxicities. This feature may imply an advantage in terms of drug metabolism, since none of the frameworks that constitute any of the complexes **1–4** (ligand and Cu(II) ion) do separately exhibit cytotoxicity. We hypothesise that, together with the

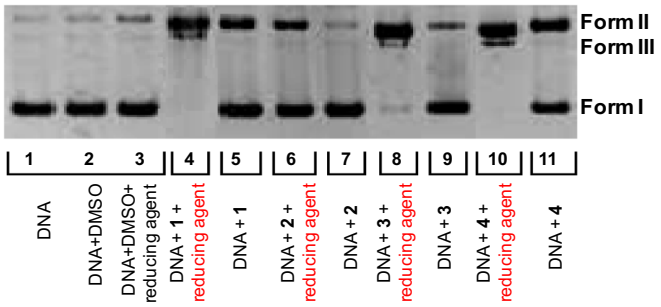

Fig. 2. Agarose gel electrophoresis of a BlueScript supercoiled plasmid DNA (ScdsDNA) treated with complexes **1**–**4** (lanes 4–11). Incubation time was 24 h at 37 °C, at a concentration of 50 μM of the complexes in NaCl/Tris-HCl (pH 7.20) buffer media. Some samples were incubated for an additional hour in the presence of a reducing agent (ascorbic acid, 100 μM): lanes 4, 6, 8, and 10. DNA controls are as follows: lane 1, pure BlueScript plasmid DNA; lane 2, pure plasmid with 10% dmso and lane 3, pure plasmid with 10% dmso and ascorbic acid (100 μM).

lower toxicity profile generally found in fibroblasts (as a proof-of-concept of non-cancer cell lines), this might lead to fewer side-effects, and hence to an ideal "softer" chemotherapy.

2.2. DNA cleaving experiments

Metallic complexes have been observed to interact with many different targets, and Cu(II) complexes are not an exception. While Pt complexes can covalently bind to *N*-donor centers in the DNA, as cisplatin does [1], copper and its complexes have shown several modes of action. Besides DNA intercalation or groove binding [16], ROS generation or superoxide dismutase (SOD) mimetic activity, among others, are examples of the reactivity observed for some of the current reported Cu(II) complexes [43,44].

DNA is still widely considered as the main target in chemotherapy. Therefore, DNA cleaving properties of complexes **1**–**4** were investigated by following the conversion of supercoiled circular plasmid DNA to opened DNA forms. The individual complexes (**1**–**4**) were incubated with a BlueScript supercoiled plasmid DNA (ScdsDNA) for 24 h and submitted to electrophoresis (Fig. 2). Complexes **1**, **3**, and **4** possess cleaving effect towards the DNA plasmid, opening the ScdsDNA (form I) and leading to its open circular DNA form (ocDNA, form II). In addition, a new band appears between forms I and II, which is ascribed to the form III (linear form) that is produced after breakage of both DNA strands.

The presence of reductants such as ascorbic acid simulates the reducing environment inside the majority of the cellular compartments. The generation of Cu(I) stimulates the potential formation of ROS, which show DNA cleaving abilities [15]. Interestingly, the complexes with the lowest IC_{50} values (**1**, **3** and **4**, Table 1) are able to totally transform ScdsDNA into ocDNA and its linear form (form III) when incubated with ascorbic acid (Fig. 2, lanes 4, 6, 8, and 10). Total vanishing of the band associated to form I indicates a strong cleaving capability under this reducing environment. This clearly points to a redox-dependent mechanism, triggered by the presence of ascorbic acid, which promotes Cu(I) generation and the potential formation of oxygen species, causing DNA damage. The cleaving capacity of complex **2** clearly differs from the rest of the assayed compounds. It resulted to be the lowest one (Fig. 2, lanes 6 and 7), not being able to totally transform ScdsDNA into ocDNA or the linear form at a concentration of 50 μM, even in the presence of ascorbic acid. This suggests that the high IC_{50} values obtained for complex **2** might be partially attributed to a poor DNA cleaving ability.

2.3. DNA binding studies

The interactions between DNA and metal complexes can be generally classified as covalent or non-covalent. The formation of DNA-complex adducts, like those reported for cisplatin and other Pt compounds [1,5], can be studied by means of several techniques, among them NMR, inductively coupled plasma optical emission spectrometry (ICP-OES), fluorescence, UV–Vis absorption and Mass Spectrometry (MS). The latest has emerged as a powerful tool to study the covalent binding between DNA and other compounds and several examples can be found in the literature [5,45,46].

In our particular case, and following the same procedure as that reported by Samper et al. [5], double-stranded oligonucleotides (DS, as a model of DNA, formed by complementary single strands OP1 and OP2) were incubated with complexes **1**–**4** at different ratios. The mass spectra recorded after those incubations (Fig. S4) do not show any peak related to the covalent binding of any of the copper compounds with the DS or the single strands (OP1, OP2). The incubation of DS with complexes **1** and **2** clearly decreases the intensity of the DS peak while those of OP1 and OP2 increase, suggesting a partial unfolding of the DS due to the presence of these complexes. On the other hand, compounds **3** and **4** promote the formation of peaks attributed to the degradation of OP1, OP2 and DS (mainly related to oxidation of the nucleic acid chains) without significant unfolding of the double stranded form.

These results indicate that the four studied complexes do not bind to DNA by covalent interactions. Three main classes of non-covalent DNA interactions have been proposed for metal complexes: intercalation, groove binding, and electrostatic interactions due to the negatively charged phosphate backbone [47,48]. In light of this, UV–Vis absorption spectroscopy was used to assess the metal complex-DNA interactions and their likely nature. The study is based on the changes on the absorbance (typically metal-to-ligand charge transfer (MLCT) absorptions and π-π* ligand transitions) upon increasing additions of calf-thymus DNA (ct-DNA) to a solution of the corresponding metal complexes. Absorption spectra in the range of 225–550 nm were recorded at a constant complex concentration (25 μM) with increasing amounts of ct-DNA. Results for complexes **1**, **2**, and **4** (Fig. 3) clearly show a hypochromic effect upon DNA addition but no significant bathochromism is observed in any spectra. This suggests an interaction with DNA *via* groove binding or electrostatic interactions rather than *via* intercalation [47,49–51].

Compounds showing high DNA intercalating properties do normally produce red-shift due to their π-π interactions with the aromatic bases of DNA [47,48], an effect that has not been observed in this case. The two other ways of interaction would be actually favoured by the opposite electrical charges of the metal compound (cations) in front of the negatively-charged DNA phosphate backbone. In the case of complex **3**, the UV–Vis spectra (Fig. 3) point to a lower interaction with ct-DNA than that observed for the other assayed compounds, confirming that it does not interact *via* intercalation either. The spectrum initially experiences ~ 5% of hyperchromic effect (up to 10 μM DNA), suggesting that it might firstly bind DNA through electrostatic interactions (external binding), whereas further additions of DNA (from 10 to 35 μM DNA) cause the decrease of the intensity in the absorbance, thus pointing to groove-binding mode [47]. The extent of the interactions of the studied complexes with DNA can be estimated based on the magnitude of the hypochromicity (Table 2). By comparing all the spectra, complex **2** shows, especially on its MLCT bands, the highest hypochromicity (15%), hence exhibiting the strongest non-covalent interaction, most probably owing to its almost totally planar structure in solution, as concluded from its EPR spectrum (Fig. S1). Complexes **1** and **4** also show similar hypochromism effects, at their absorbance maxima at 245, 266 and 293 nm. These values suggest a significant DNA interaction, most likely reinforced by the global positive charged of both compounds. On the other hand, complex **3** has the lowest hypochromicity, indicating poor DNA binding abilities.

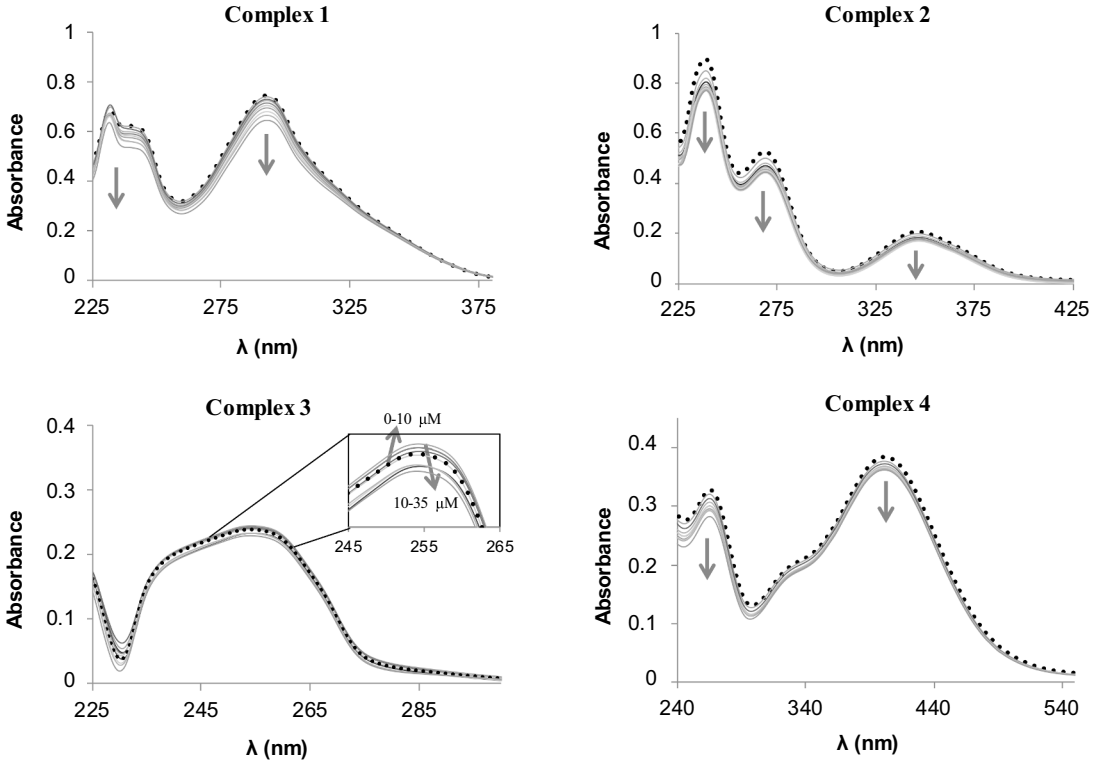

Fig. 3. Absorption spectra of complexes **1–4** (25 μM) in a NaCl (50 mM)/Tris-HCl (5 mM) buffer (pH 7.20) upon addition of calf-thymus DNA (0–35 μM). Each spectrum was recorded after 15 min of stabilization time. The arrows indicate change upon increasing concentrations of ct-DNA. Dashed line refers to the initial absorbance for each complex (0 μM ct-DNA). Data have been corrected with a DNA blanks for each concentration and for the dilution effects.

Table 2
Intrinsic binding constants (K_b) and hypochromism for the interaction of ct-DNA and complexes **1–4**. K_b is obtained from the ratio of the intercept to the slope, according to the Benesi-Hildebrand equation (Eq. (1)) [47], after the fitting of the UV–Vis data from Fig. 3 (Fig. S5).

Complex	K_b[a] (M^{-1})	log K_b	% hypochromism (λ in nm)
1	$(6.9 \pm 0.9)\cdot10^4$	4.8	12 (245), 14 (293)
2	$(5.5 \pm 1.5)\cdot10^5$	5.7	15 (238), 12 (269)
3	Non-linear fitting	–	From 10 to 35 μM: 6 (253)
4	$(1.3 \pm 0.3)\cdot10^5$	5.1	12 (266), 4 (402)

[a] The calculated K_b values from Eq. (1) arise from an approximated DNA-drug model and hence, they should be compared in orders of magnitude, rather than with the exact numbers.

Quantitative data can be obtained from the recorded absorption spectra using the Benesi-Hildebrand equation (Eq. (1)) that allows to calculate the intrinsic binding constant: K_b (Table 2). A_o is the absorbance of the complex in the absence of DNA, A is the absorbance at any given DNA concentration, and ε_G and $\varepsilon_{H\text{-}G}$ are the extinction coefficients of the complex and the complex-DNA, respectively [47,52].

$$\frac{A_o}{A - A_o} = \frac{\varepsilon_G}{\varepsilon_{H-G} - \varepsilon_G} + \frac{\varepsilon_G}{\varepsilon_{H-G} - \varepsilon_G} \cdot \frac{1}{K_b\,[DNA]} \quad (1)$$

The plot of the relative variation of the absorbance ($A_0/(A - A_0)$) *vs.* the inverse of the DNA concentration (*1/[DNA]*) allows the determination of K_b (Table 2 and Fig. S5). For complex **3**, no linear correlation could be observed and thus K_b could not be determined. The values obtained for complexes **1**, **2**, and **4** are in the order of 10^4–10^5, lower than the values around 10^6–10^7 known for classical and strong metallointercalators (4′,6-diamidino-2-phenylindole (DAPI), HOECHST, *etc.*) [47,53,54]. These values confirm moderate DNA binding affinity. Interestingly, and although complex **2** has not shown significant cytotoxic effect (Table 2), it possesses the highest binding constant, probably due to its planar geometry and π-conjugated system, which could favour groove binding interactions.

2.4. Fluorescence experiments: Ethidium bromide displacement studies

When ethidium bromide (EB, a well-known fluorescent DNA-intercalating agent) binds DNA, the fluorescence of the EB-DNA adduct increases almost 20-fold with respect to free EB. Therefore, intercalation competitive assays can be carried out by monitoring the changes of the typical EB-DNA fluorescence band at 610 nm upon increasing additions of the compound. Any intercalating molecule that competes and displaces EB from the DNA sites (in a concentration-related process) will generate a decrease in the intensity at 610 nm. Nevertheless, chemical compounds altering the DNA structure and changing its conformation, for instance by elongating or shortening it, may also cause EB discomfort and liberation [55]. EB displacement assays of complexes **1–4** have been performed to confirm the hypothesis that they should not possess intercalating properties, as shown by the DNA-complex UV–Vis studies (Fig. 3). Complexes **1–3** do not induce significant variations on the intensity of the EB-DNA fluorescence band (Fig. S6), suggesting negligible DNA conformational changes and confirming their poor intercalative abilities. However, complex **4** clearly decreases the EB-DNA band intensity (Fig. 4A). In this case, its non-planar structure in solution may induce destabilization of the DNA structure or enough conformational change to force EB displacement from its DNA binding site, rather than intercalation. In agreement with this, no red-shift was observed in the UV–Vis experiments either (Fig. 3). Considering the high antiproliferative activity observed (Table 1) as well as its high cleaving effect (Fig. 2), the DNA conformational alterations induced by complex **4**, might contribute to promote cell-death too.

Determination of the Stern-Volmer constant (K_{SV}) for complex **4** has been performed by using Eq. (2). I and I_0 are the emission intensities at 610 nm in the presence and absence of complex, respectively. A K_{SV} of $8.4\cdot10^3\ M^{-1}$ for complex **4** can be calculated by the linear fitting of the

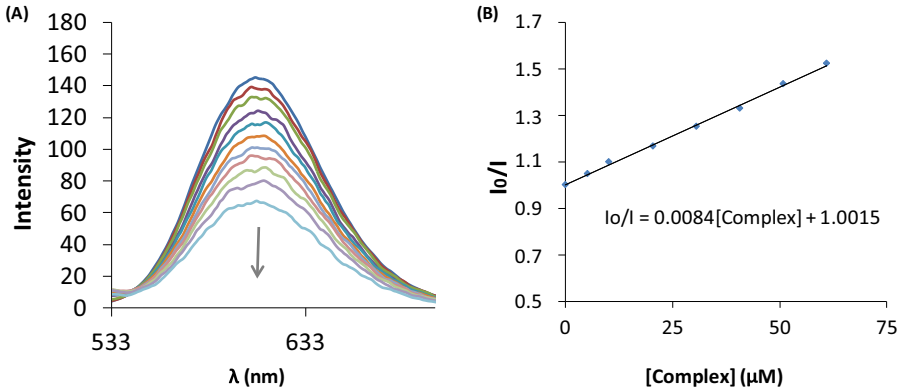

Fig. 4. (**A**) Fluorescence spectra (λ_{exc} = 514 nm and λ_{em} = 610 nm) of EB (12.5 μM) bound to ct-DNA (2.5 μM) [51] upon addition of increasing concentrations of complex **4** (0–70 μM). The data have been corrected with a dmso blank and for the dilution factors. The arrow shows increasing additions of the complex. (**B**) Plot of the I_0/I ratio *vs.* the concentration of complex **4**. K_{SV} corresponds to the slope of the linear fitting of the data according to Stern-Volmer equation (Eq. (2)).

data (Fig. 4B). Even though this value confirms some ability to displace EB from its DNA sites, it is lower than the reported values for other described Cu(II) compounds, which are, for instance, about 10^4–10^5 M^{-1} [56,57].

$$\frac{I_o}{I} = 1 + K_{SV}[Complex] \quad (2)$$

2.5. Cyclic voltammetry studies: understanding the Cu(II)/Cu(I) redox pair

Since one of the cell-death pathways reported for Cu(II) complexes implies oxidative damage [58], and the results of the DNA cleavage experiments suggest an ascorbic acid-dependent (*i.e.* redox dependent) DNA cleavage activity (Fig. 2), studying the redox properties for the complexes **1**–**4** is relevant. These data can give insight into important structural-activity relationships. Cyclic voltammetry (CV) experiments were performed with both, the free ligands and their Cu(II) complexes in *N*,*N*-dimethylformamide (dmf) and dmso (Fig. S7). The associated Cu(II)/Cu(I) redox potentials are shown in Fig. 5 and Table S1. All the ligands (bm, salenH$_2$, amp, and nbda) are electroactive in the assayed range (−2 or −1.5 to 1 V *vs.* Fc^+/Fc). The new signals observed on the cyclovoltammograms after coordination of Cu(II) are ascribed to the Cu(II)⇄Cu(I) processes. The Cu(II)/Cu(I) assigned potentials were confirmed by bulk electrolysis and EPR experiments for complexes **1**, **3** and **4** (Fig. S8). The application of a constant reducing potential (−0.6, −0.9 and −0.6 V *vs.* Fc^+/Fc) to the initial dmso solutions of the complexes **1**, **3** and **4**, respectively, gives rise to an important decrease on the corresponding Cu(II) EPR signal (Fig. S8), supporting the reduction to Cu(I). Then, constant oxidising potentials (+0.1, −0.35 and +0.1 V *vs.* Fc^+/Fc in dmso, respectively) were applied to the reduced samples. Their recorded EPR spectra (Fig. S8) show the recovering of the X-band EPR spectra, hence indicating oxidation again to Cu(II). For complex **2**, CV experiments (Fig. S7, Table S1) were carried out to corroborate the value already reported in the literature [59].

Successive scans were performed in all cases. The lack of signal change upon the different collected scans indicates that no disproportion occurred after cycling between Cu(II) and Cu(I). The I_{pa}/I_{pc} ratio close to 1 and the calculated ΔE_p values (Table S1) suggest a quasi-reversible one-electron process. The differences between cathodic and anodic peaks are much higher than the expected 0.060 V (ΔE_p ranging from 0.137 to 0.200 V) for fully reversible redox processes, but the recorded voltammogram in the same conditions for the ferrocene (Fc^+/Fc) reference compound also displays ΔE_p around 0.100 V. The linear dependence of the peak currents I_{pc} and I_{pa} *vs.* the square root of the scan rate ($\nu^{1/2}$) is indicative of a diffusion controlled process (Fig. S9) [60].

Considering the obtained IC_{50} values as well as the data for DNA cleavage experiments (Table 1 and Fig. 2, respectively), one could infer a relationship between the redox behaviour of the complexes and their antiproliferative effect. Complexes **1**, **3**, and **4** are the most actives ones (lowest IC_{50} values) and also show high cleavage effect on ScdsDNA, especially in the presence of a reducing agent as ascorbic acid. Seemingly, these complexes possess Cu(II)/Cu(I) redox processes within the biological range of −1.1 V to 0.2 V *vs.* Fc^+/Fc (Fig. 5). On the other hand, complex 2, which shows a really low inhibition activity, *i.e.* a high IC_{50} value, has the Cu(II)/Cu(I) redox potential out of this range ($E_{½}$ = −1.7 V [59], and E_{pc} = 1.85 V, Table S1). This highly negative potential is difficult to be commonly reached in eukaryotic cytosols by the glutathione (GSH) system ($E°_{(GSH/GSSG)}$ is about −0.90/−0.95 V *vs.* Fc^+/Fc) [61–63] or the common NAD^+/NADH redox pair ($E°_{(NAD+/}$

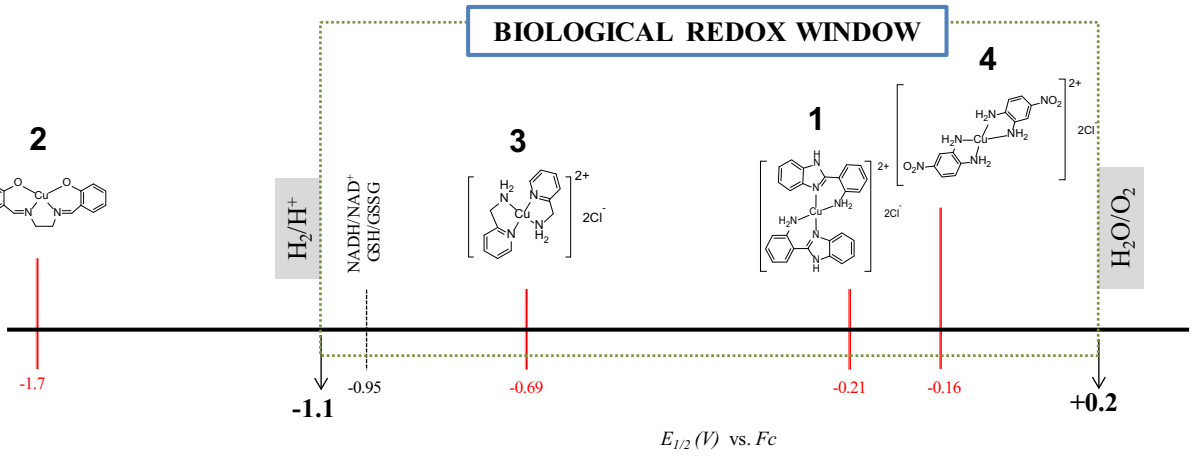

Fig. 5. Potential window for the redox chemistry of life, where complexes **1**–**4** are placed. Redox chemistry in living cells is approximately limited by the standard potentials for water oxidation and reduction at pH 7 [65].

$_{NADH)}$ = −0.95 V *vs.* Fc^+/Fc) [64]. In fact, the GSH/GSSG pair is considered one of the most important biological redox buffers in the eukaryotic systems. Therefore, reducing Cu(II) to Cu(I) in biological media is significantly less favourable for complex **2** than for **1**, **3**, and **4** (Fig. 5). This could hinder the induction of oxidative damage and, thus, imply a lower inhibition activity (Table 1). It is important to highlight that the cytotoxic activity associated to an oxidative mechanism for complexes **1–4** must be essentially attributed to the presence of the whole complex since the ligands themselves have not shown any significant cell inhibition (Table 1). These data confirm that the coordination of Cu(II) is, then, indispensable to trigger this redox-pathway. The results point to a direct relationship between the redox activity of the complexes and their effect on cell lines.

2.6. In vitro ROS generation studies: confirming the relationship of the Cu(II)/Cu(I) redox potentials with the biological activity

Results obtained in the cyclic voltammetry studies (Fig. 5) clearly suggested an oxidative dependent mechanism to trigger cell death. In order to detect the formation of intracellular ROS in HeLa cells in the presence of the complexes, the 2′,7′-Dichlorofluorescin diacetate (DCFDA) assay was performed [66,67]. DCFDA is a non-fluorescent and permeable dye that, after cleavage and oxidation by intracellular esterases and ROS, generates dichlorofluorescein (DCF), a fluorescent and non-permeable compound. For 4 h treatment, strong DCF fluorescence of up to 2-fold was observed for complexes **1**, **3** and **4** (Fig. 6) (being up to about 3-fold after 24 h), highlighting the high ROS production capabilities of these three complexes. On the contrary, complex **2** was not able to increase the ROS levels (Fig. 6) respect to the control group. This is in high agreement with the Cu(II)/Cu(I) redox potentials observed previously for the studied complexes. The ones having the Cu(II)/Cu(I) redox potential inside the biological redox windows, *i.e.* those with the thermodynamic potential of Cu(II)/Cu(I) redox cycling in cells (Fig. 5), are those generating a high ROS production level (Fig. 6) and the ones showing significant cytotoxicity (Table 1). Complex **2**, which has its Cu(II)/Cu(I) redox potential outside the biological redox window (Fig. 5), is not able to produce ROS inside HeLa cancer cells (Fig. 6) and, consequently not showing any significant cytotoxicity (Table 1).

These results confirm the strong relationship between the Cu(II)/Cu(I) redox potentials for the complexes **1–4**, their ROS production inside the cells, and their biological activity. In our systems, this reinforces the redox mechanism for Cu(II) complexes as one of the most important ones to trigger cell-death. It also emphasises the strong link between the chemical features of Cu(II) complexes and their biological activity. This

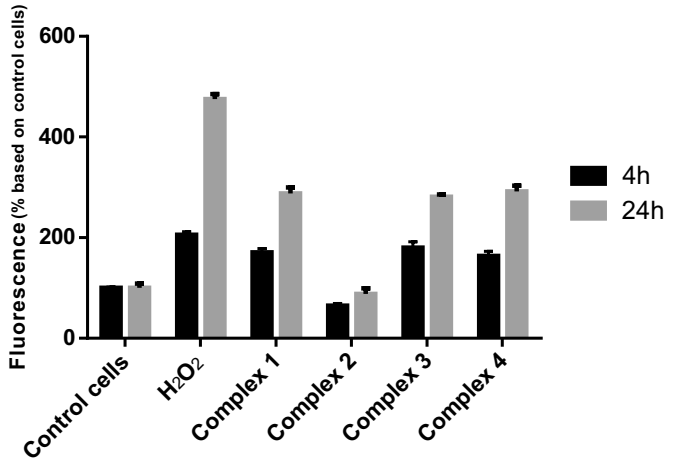

Fig. 6. ROS formation measured with the DCFDA assay in HeLa cells for complexes **1–4** at the corresponding IC_{50} values for each complex (Table 1) after treatment during 4 and 24 h. H_2O_2 (100 μM) was used as positive control.

may be used as an interesting and promising starting strategy to preliminary assess future Cu(II) complexes as anticancer drugs based on their redox features.

At this stage, some questions still remained unclear from the data here recorded. It is well known that some ligands can play redox reactions, as in complex **4**. Their versatility to expand the electron transfer reactivity of the coordinated metals beyond the mere inherent metal activity is interesting in terms of potential redox-mediated anticancer pathways, *i.e.* ROS generation [38]. Consequently, in order to examine the role of the ligand and the effect of the solvent, computational calculations have been carried out with complex **4**.

2.7. Computational approach: evaluating the role of the ligand

Mono- and bis-chelated $Cu^{II/I}$ species of complex **4**, formed by 4-nitrobenzene-1,2-diamine (nbda, Fig. 1), were examined and the structures simulated were (L = nbda): $[Cu^{II}L_2]^{2+}$, $[Cu^{II}L(dmso)_2]^{2+}$, $[Cu^{II}L(MeOH)_2]^{2+}$, $[Cu^{II}L(H_2O)_2]^{2+}$ and the respective reduced forms $[Cu^{I}L_2]^{+}$, $[Cu^{I}L(dmso)_2]^{+}$, $[Cu^{I}L(MeOH)_2]^{+}$ and $[Cu^{I}L(H_2O)_2]^{+}$. Concerning the bis-chelated species, the two possible isomers (named *cis* and *trans*) were also evaluated.

The Gibbs energy calculations for the dissociation reactions $CuL_2 + 2Solvent \rightleftarrows CuL(Solvent)_2 + L$ were performed and summarised in Table 3. The predicted complexes result in a square-planar geometry.

The results clearly show a different behaviour depending on the solvent. In dmso the dissociation reaction appears highly favoured while in H_2O and MeOH the calculations demonstrate a reaction close to equilibrium.

The computed standard reduction potential $E_{Cu^{II}|Cu^{I}}{}^{o}$ for the reaction of the Cu complex containing the dmso molecules as ligands, $[Cu^{II}(L)(dmso)_2]^{2+} + e^- \rightleftarrows [Cu^{I}(L)(dmso)_2]^{+}$, results in −0.06 V *vs.* Fc^+/Fc, close to the experimental value of −0.16 V. During the reduction reaction the Cu(II) complex undergoes a geometry distortion and a partial dissociation, as shown in Fig. 7A and B, moving from a tetra-coordinated square-planar (typically favoured for the Cu(II) moieties) to a tri-coordinated trigonal geometry (typical for Cu(I) centers).

In order to investigate the nature of the redox process, the oxidation state of the metal and the possible non-innocent behaviour of the nbda ligand, further DFT calculations were carried out considering the reduction of the ligand: $[Cu^{II}(\mathbf{L})(dmso)_2]^{2+} + e^- \rightleftarrows [Cu^{II}(\mathbf{L}\cdot^-)(dmso)_2]^{+}$. The Gibbs free energy comparison between the two species (36.8 kcal mol^{-1}) clearly shows that the ligand participation to the redox processes is negligible and the oxidation state of Cu in the two minima can be described as +II and + I. Looking at the spin density of the Cu^{II} triplet complex the acquired electron is localised on the nitro group: 0.20, 0.21, and 0.21 respectively on the O, O and N atoms (Tables S2 and S3). The structure of the radical $[Cu^{II}(\mathbf{L}\cdot^-)(dmso)_2]^{+}$ complex, as shown in Fig. 7C, remains square planar in a very similar geometry to the oxidised form (Fig. 7A).

The standard reduction potential *versus* Fc^+/Fc of the couple nbda/nbda$\cdot^-$ was also simulated, and the computed value (0.15 V) was in the range of the experimental value of 0.30 V. In this case, in analogy with the $[Cu^{II}(\mathbf{L}\cdot^-)(dmso)_2]^{+}$ complex, the acquired electron is essentially localised on the nitro group: 0.22 and 0.30 respectively on both oxygen atoms and the nitrogen (Tables S2 and S3).

The effect of the nitro group was evaluated simulating the redox process for the reaction $[Cu^{II}(\mathbf{L'})(dmso)_2]^{2+} + e^- \rightleftarrows [Cu^{I}(\mathbf{L'})(dmso)_2]^{+}$ where **L′** = benzene-1,2-diamine (bda). The computed standard reduction potential $E_{Cu^{II}|Cu^{I}}{}^{o}$ results −0.45 V *vs.* Fc^+/Fc (Table S4). For this model the triplet state results unstable, and consequently the DFT optimization was not possible. The standard reduction potential of the couple bda/bda$\cdot^-$ was also simulated and results in −4.44 V *vs.* Fc^+/Fc (Table S4). In this case, the acquired electron is completely delocalised on the benzene ring.

These data confirm that, even if the nbda ligand has no role in the

Table 3
ΔE and Δ*G* values for the dissociation of Cu^{II}-nbda bis-chelated ($[Cu^{II}L_2]^{2+}$) complexes in different solvents.[a,b]

	$[Cu^{II}L_2]^{2+}$	Solv	ΔE_{solv}	ΔG_{solv}
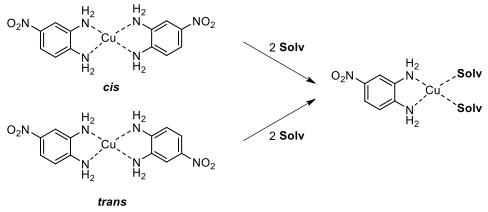	*cis*	dmso	−19.4	−8.1
	trans	dmso	−19.7	−6.9
	cis	H_2O	−12.1	−3.4
	trans	H_2O	−11.8	−3.2
	cis	MeOH	−11.5	0.7
	trans	MeOH	−11.8	0.3

[a] Values reported in kcal mol^{-1}.
[b] The correction of RTlnV (1.89 kcal mol^{-1}) was applied.

acquired electron by the full complex, the presence of the nitro group in the ligand favours the reduction of Cu(II) to Cu(I) (from −0.45 V with the bda ligand to −0.06 V *vs.* Fc^+/Fc with the nitro group, nbda ligand).

3. Conclusions

In summary, the work reported delved into the study of the anticancer properties of a series of existing Cu(II) compounds. It has been demonstrated that "old" Cu(II) complexes, previously designed for a different purpose, can offer "new" medicinal applications. This could be useful to provide potential solutions and open a new and simpler approach in anticancer therapies. This study has allowed to unveil interesting chemotherapeutic properties of complexes **1**, **3**, and **4**, specially the latter two, which possess prominent cytotoxicity in HeLa and MCF7 cells at similar and lower $IC_{50,24h}$ values than cisplatin, respectively. Moreover, their lower toxicity profile in non-cancer fibroblasts cell line enhance the potentiality of these compounds to offer less side-effects and to be furtherly tested *in vivo*. It is noteworthy to highlight the promising activity shown by complex **4**. Furthermore, examination and elucidation of their mechanism of action and their affinity towards DNA have been carried out by using several techniques. Complexes **1**, **3**, and **4** interact with DNA, showing affinity as groove binders, and they also exhibit DNA cleavage activity, basically through an oxidative mechanism. Interestingly, cyclic voltammetry measurements evidence that their activity can be strongly related to their redox behaviour, allowing to understand their oxidative mechanism of action and to establish a putative correlation between their biological activity and their coordination features. Remarkably, complexes **1**, **3** and **4** have the associated Cu(II)/Cu(I) redox potentials in a biologically available redox range and they have shown prominent cytotoxicity properties. Their chemical features correlate with their *in vitro* ROS production in HeLa cells. Complex **2** has its Cu(II) ⇄ Cu(I) redox process outside the biological window range, hence impairing any redox-mediated cell-death mechanism.

Our results reinforce the importance of the oxidative mechanism of action among the different cell-death pathways for copper complexes. This relationship can serve as a good starting point to preliminary assess potential Cu(II) anticancer drugs based on their chemical properties and to improve some existing metal-based drugs. Theoretical calculations supported the importance of the metal-centered Cu(II)/Cu(I) redox reaction as well as the variation of the redox properties with the interaction with the solvent.

4. Experimental section

4.1. Materials and methods

Chemicals were purchased from commercial suppliers and used as received. Copper(II) chloride, copper(II) acetate, 2-(2-aminophenyl)-1*H*-benzimidazole (bm), 2-(aminomethyl)pyridine (amp), 4-nitrobenzene-1,2-diamine (nbda), 2′,7′-dichlorofluorescin diacetate (DCFDA), and calf-thymus DNA sodium salt (ct-DNA) were obtained from Sigma-Aldrich. Solvents (acetonitrile (ACN), methanol (MeOH),

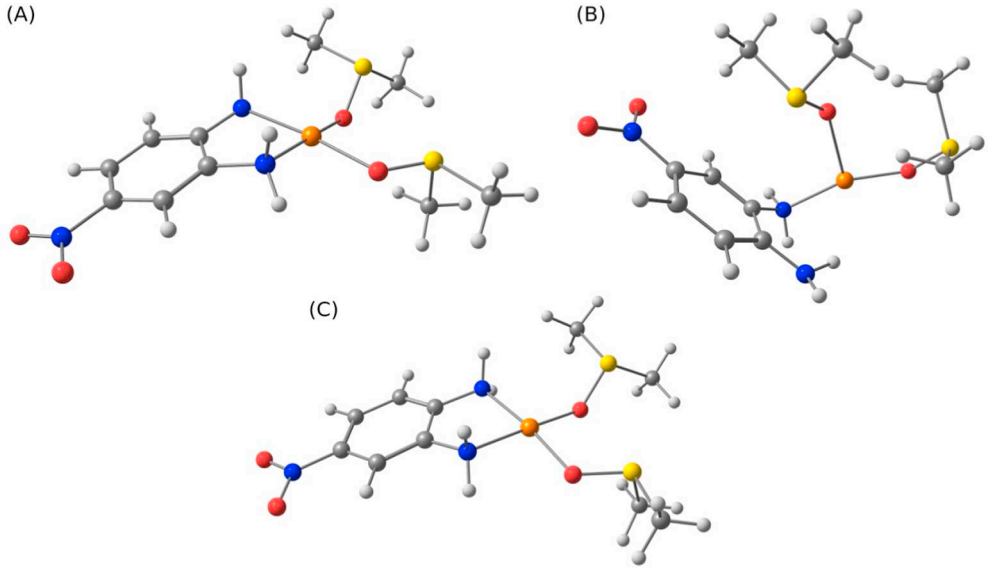

Fig. 7. Optimized geometry of the complexed species: (A) $[Cu^{II}(\mathbf{L})(dmso)_2]^{2+}$, (B) $[Cu^{I}(\mathbf{L})(dmso)_2]^{+}$. and (C) $[Cu^{II}(\mathbf{L}\cdot^{-})(dmso)_2]^{+}$.

ethanol (EtOH), chloroform ($CHCl_3$), dimethyl sulfoxide (dmso), *N*,*N*-dimethylformamide (dmf), and dichloromethane (DCM)) were used at synthesis grade purity and directly from commercial sources (Scharlab). DNA oligonucleotides sequences (OP1 and OP2 sequences: 5′-CACTTC CGCT-3′ and 5′-AGCGGAAGTG-3′, respectively) were purchased from EUROFINS MWG Synthesis GmbH supplier.

4.2. Copper complexes synthesis

4.2.1. $[Cu(bm)_2]Cl_2$ (complex 1)

This complex was synthesized adapting reported procedures [32]. To a solution of $CuCl_2{\cdot}2H_2O$ (0.24 mmol, 1.0 eq) in ACN (5 mL), a solution of 2-(2-aminophenyl)-1*H*-benzimidazole (bm) (0.44 mmol, 1.9 eq) in ACN (30 mL) was added. The mixture was stirred for 2 h at room temperature and stored at −30 °C for 1 h. The resultant precipitate was filtered off, washed with ACN and dried under vacuum to obtain the brown solid **1** (74% yield). HR-MS (ESI+, MeOH-$CHCl_3$): *m/z* = 480.1116 (calc. for $[1\text{-H-2Cl}]^+$ = 480.1118). Analysis calc. for $[Cu(bm)_2]Cl_2{\cdot}2H_2O$ ($C_{26}H_{26}Cl_2CuN_6O_2$): C, 53.02; H, 4.45; N, 14.27. Found: C, 52.83; H, 4.09; N, 14.15.

4.2.2. [Cu(salen)] (complex 2)

This complex and its salenH_2 ligand were synthesized following adapted procedures from [Co(salen)] [39]. Under nitrogen atmosphere, a solution of $Cu(OAc)_2{\cdot}H_2O$ (0.76 mmol, 1.0 eq) in MilliQ H_2O (2 mL) was added dropwise into a solution of salenH_2 (0.75 mmol, 1.0 eq) in absolute EtOH (15 mL) at 70 °C. The solution was stirred at 75 °C and under argon atmosphere for 2 h. The precipitate was filtered off and washed with H_2O and with EtOH to get a dark green solid (73% yield). HR-MS (ESI^+, MeOH-$CHCl_3$): *m/z* = 352.0242 (calc. for $[\mathbf{2} + Na]^+$ = 352.0243). Elemental analysis calc. for [Cu(salen)] ($C_{16}H_{14}CuN_2O_2$): C, 58.26; H, 4.28; N, 8.49. Found: C, 57.84; H, 4.33; N, 8.48.

4.2.3. $[Cu(amp)_2]Cl_2$ (complex 3)

This complex was synthesized as described elsewhere [35]. To a solution of $CuCl_2{\cdot}2H_2O$ (0.32 mmol, 1.0 eq) in ACN (15 mL), 2-(aminomethyl)pyridine (amp) (0.58 mmol, 1.8 eq) was added. The resulting solution was stirred overnight at room temperature. The blue precipitate was filtered off, washed with ACN and DCM, and dried under vacuum to get the blue solid **3** (80% yield). HR-MS (ESI^+, MeOH): *m/z* = 314.0349 (calc. for $[\mathbf{3}\text{-Cl}]^+$ = 314.0354). Analysis calc. for $[Cu(amp)_2]Cl_2{\cdot}H_2O$ ($C_{12}H_{18}Cl_2CuN_4O$): C, 39.09; H, 4.92; N, 15.19. Found: C, 38.93; H, 5.05; N, 14.84.

4.2.4. $[Cu(nbda)_2]Cl_2$ (complex 4)

Synthesis based on reported literature [37]. To a solution of $CuCl_2{\cdot}H_2O$ (0.29 mmol, 1.0 eq) in ACN (10 mL), 4-nitrobenzene-1,2-diamine (nbda) (0.59 mmol, 2.0 eq) in ACN:DCM (5 mL, 1:0.3) was added. The resulting solution was stirred at 0 °C for 2 h. The precipitate was filtered off, washed with ACN and DCM, and dried under vacuum to yield the green solid **4** (55% yield). HR-MS (ESI^+, MeOH): *m/z* = 368.0273 (calc. for $[\mathbf{4}\text{-H-2Cl}]^+$ = 368.0289). Analysis calc. for $[Cu(nbda)_2]Cl_2$ ($C_{12}H_{14}C_{l2}CuN_6O_4$): C, 32.70; H, 3.20; N, 19.07. Found: C, 32.98; H, 3.22; N, 18.97.

4.3. HR ESI-MS measurements

Routine HR ESI-MS measurements were recorded after diluting the corresponding solid complexes in dmso:MeOH 1:10 in a MicroTOF-Q (Brucker Daltonics GmbH, Bremen, Germany) instrument equipped with an electrospray ionization source (ESI) in positive mode. Conditions were those used in routine experiments. The nebulizer pressure was 1.5 Bar, the desolvation temperature was 180 °C, dry gas at 6 L min^{-1}, the capillary counter-electrode voltage was 5 kV and the quadrupole ion energy, 5.0 eV.

4.4. DNA-drug covalent binding assays

Covalent interactions were studied using ESI-MS spectrometry in negative mode and following a reported procedure in our group [5]. OP1 and OP2 were heated together up to 70 °C and cooled down slowly to room temperature to yield the double-stranded oligonucleotide (DS). Complexes **1**–**4** were incubated for 24 h at 37 °C with the DS (20 μM) in 1:5 or 1:20 ratios (DS:complex) in 25 mM NH_4HCO_3 buffer (pH 7.20) containing a maximum of 5% dmso to dissolve them.

4.5. EPR experiments

Electron paramagnetic resonance measurements were carried out on a BRUKER ELEXSYS 500 X-band CW-EPR spectrometer, with an ELEXSYS Bruker instrument equipped with a BVT 3000 digital temperature controller. The spectra were recorded at 120 K in frozen dmso solutions otherwise noticed. Simulations with automatic parameter fitting were performed for axial symmetry using a published software [68]. The contribution of naturally abundant ^{63}Cu and ^{65}Cu was considered, but the values given refer to ^{63}Cu. All principal axes were supposed parallel. Typical parameters were: microwave power 10–20 mW, modulation frequency 100 kHz, modulation gain 3 G.

4.6. Cyclic voltammetry

Cyclic voltammograms were taken on a BioLogic SP-150 potentiostat and EC-Lab 5,40 software. Dmso and dmf were used as solvent with 0.1 M of $[NBu_4][PF_6]$ (TBAP) as supporting electrolyte. In these conditions, the $E_{1/2}$ value for complex **2** could only be obtained in dmf due to its wider working redox window than dmso. $E_{1/2}$ value in dmso was extracted from the literature [59]. Measurements were carried out with a three electrode configuration cell: glassy carbon electrode as working electrode, Ag wire in a 0.1 M TBAP solution in dmso or dmf as reference and Pt as the counter electrode. Ferrocene (Fc^+/Fc) system was used as internal standard. The scan rate (ν) varied between 500 and 25 mV·s^{-1}. All the experiments were recorded under argon atmosphere.

4.7. Elemental analysis

C, H, O analyses were performed on a Flash EA 2000 CHNS Thermo Fisher Scientific equipment, with a TCD and a MAS 200 R autosampler for solid samples.

4.8. UV–Vis studies

Non-covalent DNA-complex interactions were studied by UV–Vis measurements. All the spectra were recorded at room temperature on an Agilent HP 8453 UV–Vis spectrophotometer in 1-cm quartz cuvettes. Solutions of complexes **1**–**4** were prepared in 50 mM NaCl/5 mM Tris-HCl buffer (pH 7.20), containing a maximum of 2% dmso to solubilize them. Ct-DNA stock solutions were prepared from its corresponding sodium salt (Sigma Aldrich) and the concentration determined from its absorbance at 260 nm (ε = 6600 cm^{-1}). Blank and dilution effects were corrected using the GRAMS32 software.

4.9. Fluorescence measurements

DNA intercalation properties of complexes **1**–**4** were studied on a Perkin Elmer LS 55 50 Hz Fluorescence Spectrometer, connected to a PC system and a water bath temperature controller. The experiments were performed at a constant temperature of 20 °C on disposable poly(methyl-methacrylate) (PMMA) cuvettes (d = 1 cm). EB-DNA (ct-DNA) samples were prepared in 50 mM NaCl/5 mM Tris-HCl buffer medium (pH 7.20). Cu complexes were added to the EB-DNA sample in dmso solution (reaching a maximum of 2% of dmso in the final mixture). Each spectrum was collected after 15 min of stabilization.

4.10. DNA cleaving experiments

Gel electrophoresis experiments were performed on agarose gel (1% in TAE buffer, Tris-Acetate EDTA), using a BIORAD horizontal tank connected to variable potential power supply. Samples were stained with EB and revealed with a Super GelDoc PlusImager. Complexes **1–4** were incubated with the Plasmid DNA (200 ng of BlueScript plasmid per well) in 20 mM NaCl/40 mM Tris-HCl buffer (pH 7.20) medium for 24 h at 37 °C (< 10% dmso in the final mixture to solubilize the complexes). Samples containing the reducing agent ascorbic acid were incubated for 1.5 extra hours in the presence of ascorbic acid (100 μM).

4.11. Cell-viability assays

The IC_{50} values were evaluated using PrestoBlue Cell Reagent (Life Technologies) assay. Stock solutions for the complexes **1–4** were freshly prepared in dmso and diluted with DMEM medium for working concentrations (final amount < 0.1% dmso in biological experiments). Human cancer cells (HeLa, MCF7 and CCD112CoN) were obtained from American Type Culture Collection (ATCC, Manassas, VA, USA). The cells were routinely cultured with DMEM (Dubbeco's modified Eagle's medium, Invitrogen) containing 10% heat-inactivated fetal bovine serum (FBS) at 37 °C in a humidified CO_2 atmosphere. HeLa cells were plated at a density of $3{\cdot}10^3$ cells/well in 100 μL of culture medium and allowed to grow overnight. After 24 h incubation with different concentrations (0, 10, 25, 50, 100, or 200 μM) of each complex, 10 μL of PrestoBlue® were added following the standard protocol. The fluorescence of each well was measured at 572 nm with a Microplate Reader Victor3 (Perkin Elmer). The relative cell viability (%) for each sample related to the control well was calculated. Each complex was tested per triplicate and averaged from three independent set of experiments. Blank and complex controls were also considered.

4.12. ROS production assays

HeLa cells were plated, grown and allowed to adhere overnight in a 96-wells plate ($20{\cdot}10^3$ cells/well). The 2′,7′-dichlorofluorescin diacetate reagent (DCFCDA, 25 μM in dmso) was then added and the cells incubated at 37 °C in the dark for 30 min. The DCFDA solution was removed and cells were treated with complexes at the corresponding IC_{50} values (at 72 h) measured for each complex and incubated for 24 h. The experiments were run in triplicate. H2O2 was used as a positive control at 100 μM. The fluorescence of each well was measured at 535 nm with a Microplate Reader Victor3 (Perkin Elmer) after excitation at 485 nm.

4.13. Computational details

The geometry of Cu^{II} complexes $[Cu^{II}L_2]^{2+}$, $[Cu^{II}L(DMSO)_2]^{2+}$, and $[Cu^{I}L_2]^{+}$, $[Cu^{I}L(DMSO)_2]^{+}$, complexes were optimized with Gaussian09 [69] at DFT level of theory with the hybrid B3LYP functional combined with the Grimme's D3 correction [70] for dispersion and the split-valence plus polarization function 6-31 g(d,p) basis-set for the main group elements while, SDD plus *f*-functions [71] and pseudopotential were applied for copper. The effect of solvation was taken into account using the SMD continuum model of Marenich et al. [72] For all the structures, minima were verified through frequency calculations.

The stability calculations were estimated computing the Gibbs free energy change in implicit solvent continuum model. The Gibbs Free Energy of the reduction reactions in solution ($\Delta G_{aq}^{0,\ RedOx}$) was computed as $\Delta G_{aq}^{o,\ Ox|Red} = \Delta G_{sol}^{o}(Red) - \Delta G_{sol}^{o}(Ox)$ assuming $\Delta G_{sol}^{o}(e^-)$ equal to zero [73]. The previous optimized geometry of the Cu(II) complexes $[Cu^{II}(\mathbf{L})]^{2+}$ and $[Cu^{II}(\mathbf{L})(DMSO)_2]^{2+}$ were re-optimized considering the charge and multiplicity relative to the $[Cu^{I}L_2]^{+}$, $[Cu^{I}L(DMSO)_2]^{+}$ forms. The standard redox potential *versus* the SHE was calculated as:

$$E_{Ox|Red}^{o} = -\left(\frac{\Delta G_{aq}^{o,Ox|Red} - \Delta G_{SHE}^{o}}{F}\right)$$

where F is the Faraday constant (96.485 $kJ{\cdot}V^{-1}{\cdot}mol^{-1}$). The widely accepted value of the half-cell proton reduction, $\Delta G_{SHE}^{o} = -427.43\ kJ{\cdot}mol^{-1}$ was used [73]. Since the experimental voltammograms have been recorded *vs* the Fc^{+}/Fc reference electrode at 25 °C, the theoretical reduction potentials were converted to the same reference by subtraction of 0.68 V [74] (Tables S2 and S4).

The Gibbs Free Energy of the reduction reactions for the organic ligands were computed increasing the basis-set to 6-311 + + G (d,p). For the Cu complexes, the Gibbs energies were computed by addition of the thermal and entropic corrections (G^{therm}), obtained in the optimization stage, to the potential energy of single point calculations with the extended basis-set 6-311 + + G(2d,p) for the main group elements [71] and the quadruple-ζ *def2*-QZVP basis set for Cu [75,76].

Abbreviations list

Amp	2-(aminomethyl)pyridine
Bm	2-(2-aminophenyl)-1*H*-BenziMidazole
Nbda	4-Nitrobenzene-1,2-diamine
SalenH2	*N,N′*-bis(salicylidene)ethylenediamine
ROS	Reactive Oxygen Species
DS	Double Stranded
SOD	Superoxide dismutase
ct-DNA	Calf-thymus DNA
dmso	Dimethyl sulfoxide
dmf	*N,N*-Dimethylformamyde
EB	Ethidium Bromide
Fc^{+}/Fc	Ferrocenium/Ferrocene
GSH	Gluthathione

Conflicts of interest

There are no conflicts to declare.

Acknowledgements

Experimental support of Sergi Montané (Institut de Biotecnologia i Biomedicina, Dept. Bioquímica i Biologia Molecular, Universitat Autònoma de Barcelona) is kindly acknowledged. This work was supported by the Spanish Ministerio de Ciencia e Innovación and FEDER to the projects BIO2015-67358-C2-2-P, CTQ2015-70371-REDT and BIO2016-78057-R. QP acknowledges the Ministerio de Educación, Cultura y Deporte the financial support of a FPU grant. The authors from the UAB are members of the "Grup de Recerca de la Generalitat de Catalunya" ref. 2017SGR-864. The Servei d'Anàlisi Química at the UAB is also kindly acknowledged for allocating instrument time.

Appendix A. Supplementary data

Supplementary data to this article can be found online at https://doi.org/10.1016/j.jinorgbio.2019.03.011.

References

[1] Z. Guo, P.J. Sadler, Angew. Chemie Int. Ed. 38 (1999) 1512–1531.
[2] S.P. Fricker, Dalton Trans. 21 (2007) 4903–4917.
[3] H.M. Pinto, J.H. Schornagel (Eds.), Platinum and Other Metal Coordination Compounds in Cancer Chemotherapy, 2 1996 New York, NY.
[4] T. Karasawa, M. Sibrian-Vazquez, R.M. Strongin, P.S. Steyger, PLoS One 8 (2013) e66220.
[5] K.G. Samper, C. Vicente, V. Rodríguez, S. Atrian, N. Cutillas, M. Capdevila, J. Ruiz, Ò. Palacios, Dalton Trans. 41 (2012) 300–306.
[6] R.P. Perez, Eur. J. Cancer 34 (1998) 1535–1542.
[7] M. Ohmichi, J. Hayakawa, K. Tasaka, H. Kurachi, Y. Murata, Trends Pharmacol. Sci. 26 (2005) 113–116.

[8] W. Han Ang, P.J. Dyson, Eur. J. Inorg. Chem. 20 (2006) 4003–4018.
[9] G. Sava, G. Jaouen, E.A. Hillard, A. Bergamo, Dalton Trans. 41 (2012) 8226–8234.
[10] C.-T. Poon, P.-S. Chan, C. Man, F.-L. Jiang, R.N.S. Wong, N.-K. Mak, D.W.J. Kwong, S.-W. Tsao, W.-K. Wong, J. Inorg. Biochem. 104 (2010) 62–70.
[11] Z. Liu, A. Habtemariam, A.M. Pizarro, S.A. Fletcher, A. Kisova, O. Vrana, L. Salassa, P.C.A. Bruijnincx, G.J. Clarkson, V. Brabec, P.J. Sadler, J. Med. Chem. 54 (2011) 3011–3026.
[12] I. Ott, Coord. Chem. Rev. 253 (2009) 1670–1681.
[13] K.D. Mjos, C. Orvig, Chem. Rev. 114 (2014) 4540–4563.
[14] T.K. Goswami, B.V.S.K. Chakravarthi, M. Roy, A.A. Karande, A.R. Chakravarty, Inorg. Chem. 50 (2011) 8452–8464.
[15] S.M.G. Leite, L.M.P. Lima, S. Gama, F. Mendes, M. Orio, I. Bento, A. Paulo, R. Delgado, O. Iranzo, Inorg. Chem. 55 (2016) 11801–11814.
[16] C. Santini, M. Pellei, V. Gandin, M. Porchia, F. Tisato, C. Marzano, Chem. Rev. 114 (2014) 815–862.
[17] C. Marzano, M. Pellei, F. Tisato, C. Santini, Anti Cancer Agents Med. Chem. 9 (2009) 185–211.
[18] P.U. Maheswari, S. Roy, H. den Dulk, S. Barends, G. van Wezel, B. Kozlevcar, P. Gamez, J. Reedijk, J. Am. Chem. Soc. 128 (2006) 710–711.
[19] J.J.R. Fraústo da Silva, R.J.P. Williams, The Biological Chemistry of the Elements: The Inorganic Chemistry of Life, Oxford University Press, Oxford, NY, 2001.
[20] H.-B. Kraatz, N. Metzler-Nolte, Concepts and Models in Bioinorganic Chemistry, Wiley-VCH, Weinheim, 2006.
[21] S.J. Lippard, J.M. Berg, Principles of Bioinorganic Chemistry, University Science Books, Mill Valley, CA, 1994.
[22] R.R. Crichton, Biological Inorganic Chemistry. An Introduction, 2n edition, Elsevier, 2012.
[23] H. Pelicano, D. Carney, P. Huang, Drug Resist. Updat. 7 (2004) 97–110.
[24] P.T. Schumacker, Cancer Cell 10 (2006) 175–176.
[25] S.E. Allen, R.R. Walvoord, R. Padilla-Salinas, M.C. Kozlowski, Chem. Rev. 113 (2013) 6234–6458.
[26] F. Lazreg, F. Nahra, C.S.J. Cazin, Coord. Chem. Rev. 293-294 (2015) 48–79.
[27] J.L. Kurtz, G.L. Burce, D.W. Margerum, Inorg. Chem. 17 (1978) 2454–2460.
[28] J.D. Egbert, C.S.J. Cazin, S.P. Nolan, Catal. Sci. Technol. 3 (2013) 912–926.
[29] D.M. D'Souza, T.J.J. Müller, Chem. Soc. Rev. 36 (2007) 1095–1108.
[30] D.A. Evans, Marisa C. Kozlowski, Jerry A. Murry, Christopher S. Burgey, Kevin R. Campos, A. Brian T. Connell, R.J. Staples, J. Am. Chem. Soc. 121 (1999) 669–685.
[31] T. Storr, M. Merkel, G.X. Song-Zhao, L.E. Scott, D.E. Green, M.L. Bowen, K.H. Thompson, B.O. Patrick, H.J. Schugar, C. Orvig, J. Am. Chem. Soc. 129 (2007) 7453–7463.
[32] C. Rodríguez-Rodríguez, N. Sánchez de Groot, A. Rimola, A. Alvarez-Larena, V. Lloveras, J. Vidal-Gancedo, S. Ventura, J. Vendrell, M. Sodupe, P. González-Duarte, J. Am. Chem. Soc. 131 (2009) 1436–1451.
[33] H. Schugar, D.E. Green, M.L. Bowen, L.E. Scott, T. Storr, K. Böhmerle, F. Thomas, D.D. Allen, P.R. Lockman, M. Merkel, K.H. Thompson, C. Orvig, Angew. Chemie Int. Ed. 46 (2007) 1716–1718.
[34] V. C. da Silveira, J. S. Luz, C. C. Oliveira, I. Graziani, M. R. Ciriolo and A. M. da Costa Ferreira, J. Inorg. Biochem., 2008, 102, 1090–1103.
[35] C. Wang, Y. Zhang, B. Yuan, J. Zhao, J. Mol. Catal. A Chem. 333 (2010) 173–179.
[36] P.G. Cozzi, Chem. Soc. Rev. 33 (2004) 410–421.
[37] M. Salavati-Niasari, J. Mol. Catal. A Chem. 245 (2006) 192–199.
[38] D.L.J. Broere, R. Plessius, J.I. van der Vlugt, Chem. Soc. Rev. 44 (2015) 6886–6915.
[39] T.G. Appleton, J. Chem. Educ. 54 (1977) 443.
[40] U. Sakaguchi, A.W. Addison, J. Chem. Soc. Dalton Trans. (1979) 600–608.
[41] J. Peisach, W.E. Blumberg, Arch. Biochem. Biophys. 165 (1974) 691–708.
[42] J. Grau, C. Renau, A.B. Caballero, A. Caubet, M. Pockaj, J. Lorenzo, P. Gamez, Dalt. Trans. 47 (2018) 4902–4908.
[43] M.P. Cervantes-Cervantes, J.V. Calderón-Salinas, A. Albores, J.L. Muñoz-Sánchez, Biol. Trace Elem. Res. 103 (2005) 229–248.
[44] A.R. Chakravarty, P.A.N. Anreddy, B.K. Santra, A.M. Thomas, Proc. Indian Acad. Sci. - Chem. Sci. 114 (2002) 391–401.
[45] K.G. Samper, V. Rodríguez, E. Ortega-Carrasco, S. Atrian, J.D. Maréchal, N. Cutillas, A. Zamora, C. de Haro, M. Capdevila, J. Ruiz, Ò. Palacios, Biometals 27 (2014) 1159–1177.
[46] J. Ruiz, V. Rodríguez, N. Cutillas, K.G. Samper, M. Capdevila, Ò. Palacios, A. Espinosa, Dalton Trans. 41 (2012) 12847–12856.
[47] M. Sirajuddin, S. Ali, A. Badshah, J. Photochem. Photobiol. B 124 (2013) 1–19.
[48] P.C.A. Bruijnincx, P.J. Sadler, Curr. Opin. Chem. Biol. 12 (2008) 197–206.
[49] T. Pivetta, F. Isaia, G. Verani, C. Cannas, L. Serra, C. Castellano, F. Demartin, F. Pilla, M. Manca, A. Pani, J. Inorg. Biochem. 114 (2012) 28–37.
[50] V. Rajendiran, R. Karthik, M. Palaniandavar, H. Stoeckli-Evans, V.S. Periasamy, M.A. Akbarsha, B.S. Srinag, H. Krishnamurthy, Inorg. Chem. 46 (2007) 8208–8221.
[51] Ratio to fully occupy all the EB-DNA binding sites according to: R.F. Brissos, E. Torrents, F.M. dos Santos Mello, W. Carvalho Pires, E. de P. Silveira-Lacerda, A.B. Caballero, A. Caubet, C. Massera, O. Roubeau, S.J. Teat, P. Gamez, Metallomics 6 (2014) 1853–1868.
[52] H.A. Benesi, J.H. Hildebrand, J. Am. Chem. Soc. 71 (1949) 2703–2707.
[53] A.K. Williams, S.C. Dasilva, A. Bhatta, B. Rawal, M. Liu, E.A. Korobkova, Anal. Biochem. 422 (2012) 66–73.
[54] N.P. Bazhulina, A.M. Nikitin, S.A. Rodin, A.N. Surovaya, Y.V. Kravatsky, V.F. Pismensky, V.S. Archipova, R. Martin, G.V. Gursky, J. Biomol. Struct. Dyn. 26 (2009) 701–718.
[55] J.C. Peberdy, J. Malina, S. Khalid, M.J. Hannon, A. Rodger, J. Inorg. Biochem. 101 (2007) 1937–1945.
[56] R. Singh, R.N. Jadeja, M.C. Thounaojam, T. Patel, R.V. Devkar, D. Chakraborty, Inorg. Chem. Commun. 23 (2012) 78–84.
[57] X.-B. Fu, D.-D. Liu, Y. Lin, W. Hu, Z.-W. Mao, X.-Y. Le, Dalton Trans. 43 (2014) 8721–8737.
[58] R.F. Brissos, A. Caubet, P. Gamez, Eur. J. Inorg. Chem. 2015 (2015) 2633–2645.
[59] S. Zolezzi, S. Evgenia, A. Decinti, Polyhedron 21 (2002) 55–59.
[60] A.J. Bard, L.R. Faulkner, Electrochemical Methods: Fundamentals and Applications, Wiley, 2001.
[61] H.R. López-Mirabal, J.R. Winther, Biochim. Biophys. Acta 1783 (2008) 629–640.
[62] H. Østergaard, C. Tachibana, J.R. Winther, J. Cell Biol. 166 (2004) 337–345.
[63] M.C. Elvington, K.J. Brewer, R.A. Scott, C.M. Lukehart (Eds.), Applications of Physical Methods to Inorganic and Bioinorganic Chemistry, Chapter Electrochemistry, John Wiley & Sons, 2007, pp. 17–38.
[64] D. Voet, J. Voet, C. Pratt, Fundamentals of Biochemistry, 4th edition, John Wiley & Sons, New York, 2013.
[65] Figure adapted from: W.R. Hagen, Biomolecular EPR Spectroscopy, CRC Press, Taylor& Francis Group, London, 2009.
[66] C.H. Ng, S.M. Yong, Y.L. Tiong, M.J. Maah, N. Sukram, M. Ahmad, A.S.B. Khoo, Metallomics 6 (2014) 892–906.
[67] A. Battacharyya, A. Dixit, S. Banerjee, B. Roy, A. Kumar, A.A. Karande, A.R. Chakravarty, RSC Adv. 6 (2016) 104474–104482.
[68] A. Rockenbauer, L. Korecz, Appl. Magn. Reson. 10 (1996) 29–43.
[69] M. J. Frisch, G. W. Trucks, H. B. Schlegel, G. E. Scuseria, M. A. Robb, J. R. Cheeseman, G. Scalmani, V. Barone, B. Mennucci, G. A. Petersson, H. Nakatsuji, M. Caricato, X. Li, H. P. Hratchian, A. F. Izmaylov, J. Bloino, G. Zheng, J. L. Sonnenberg, M. Hada, M. Ehara, K. Toyota, R. Fukuda, J. Hasegawa, M. Ishida, T. Nakajima, Y. Honda, O. Kitao, H. Nakai, T. Vreven, J. A. Montgomery Jr., J. E. Peralta, F. Ogliaro, M. Bearpark, J. J. Heyd, E. Brothers, K. N. Kudin, V. N. Staroverov, T. Keith, R. Kobayashi, J. Normand, K. Raghavachari, A. Rendell, J. C. Burant, S. S. Iyengar, J. Tomasi, M. Cossi, N. Rega, J. M. Millam, M. Klene, J. E. Knox, J. B. Cross, V. Bakken, C. Adamo, J. Jaramillo, R. Gomperts, R. E. Stratmann, O. Yazyev, A. J. Austin, R. Cammi, C. Pomelli, J. W. Ochterski, R. L. Martin, K. Morokuma, V. G. Zakrzewski, G. A. Voth, P. Salvador, J. J. Dannenberg, S. Dapprich, A. D. Daniels, Ö. Farkas, J. B. Foresman, J. V. Ortiz, J. Cioslowski and D. J. Fox, Gaussian 09, Revision c.01. Gaussian, Inc.: Wallingford, CT, 2010.
[70] S. Grimme, J. Antony, S. Ehrlich, H. Krieg, J. Chem. Phys. 132 (2010) 154104.
[71] A. Ehlers, M. Böhme, S. Dapprich, A. Gobbi, A. Höllwarth, V. Jonas, K. Köhler, R. Stegmann, A. Veldkamp, G. Frenking, Chem. Phys. Lett. 208 (1993) 111–114.
[72] A.V. Marenich, C.J. Cramer, D. Truhlar, J. Phys. Chem. B 113 (2009) 6378–6396.
[73] P. Jaque, A.V. Marenich, C.J. Cramer, D.G. Truhlar, J. Phys. Chem. C 111 (2007) 5783–5799.
[74] N.G. Connelly, W.E. Geiger, Chem. Rev. 96 (1996) 877–910.
[75] F. Weigend, F. Furche, R. Ahlrichs, J. Chem. Phys. 119 (2003) 12753–12762.
[76] D. Sanna, V. Ugone, G. Sciortino, B.F. Parker, Z. Zhang, C.J. Leggett, J. Arnold, L. Rao, E. Garribba, Eur. J. Inorg. Chem. 2018 (2018) 1805–1816.